Impact of remineralization profile shape on the air-sea carbon balance

Jonathan Maitland Lauderdale[1] and B. B. Cael[2]

[1]Department of Earth, Atmospheric and Planetary Sciences, Massachusetts Institute of Technology, Cambridge, MA 02139, USA.

[2]Ocean Biogeochemistry and Ecosystems, National Oceanography Centre, Southampton, SO14 3ZH, UK.

Key Points:

- Six alternative flux profiles fit to a Martin curve yield large differences in atmospheric carbon.
- Structural uncertainty comprises one third of total uncertainty in the ocean's biological pump.

Plain Language Summary

The ocean's "biological pump" regulates atmospheric carbon dioxide levels and climate by transferring organic carbon produced at the surface by phytoplankton to the ocean interior via "marine snow", where the organic carbon is consumed and respired by microbes. This surface to deep transport is usually described by a power-law relationship of sinking particle concentration with depth. Uncertainty in biological pump strength can be related to different variable values ("parametric" uncertainty) or the underlying equations ("structural" uncertainty) that describe organic matter export. We evaluate structural uncertainty using an ocean biogeochemistry model by substituting six alternative remineralization profiles fit to a reference power-law curve. Structural uncertainty makes a substantial contribution, about one third in atmospheric pCO_2 terms, to total uncertainty of the biological pump, highlighting the importance of improving biological pump characterization from observations and its mechanistic inclusion in climate models.

Corresponding author: JML, jml1@mit.edu

Corresponding author: BBC, cael@noc.ac.uk

Abstract

The ocean's "biological pump" significantly modulates atmospheric carbon dioxide levels. However, the complexity and variability of processes involved introduces uncertainty in interpretation of transient observations and future climate projections. Much work has focused on "parametric uncertainty", particularly determining the exponent(s) of a power-law relationship of sinking particle flux with depth. Varying this relationship's functional form introduces additional "structural uncertainty". We use an ocean biogeochemistry model substituting six alternative remineralization profiles fit to a reference power-law curve, to characterize structural uncertainty, which, in atmospheric pCO_2 terms, is roughly 50% of the parametric uncertainty associated with varying the power-law exponent within its plausible global range, and similar to uncertainty associated with regional variation in power-law exponents. The substantial contribution of structural uncertainty to total uncertainty highlights the need to improve characterization of biological pump processes, and compare the performance of different profiles within Earth System Models to obtain better constrained climate projections.

1 Introduction

Carbon and nutrients are consumed by phytoplankton in the surface ocean during primary production, leading to a downward flux of organic matter (Fig. 1). This "marine snow" is transformed, respired, and degraded by heterotrophic organisms in deeper waters, ultimately releasing those constituents back into dissolved inorganic form. Oceanic overturning and turbulent mixing returns resource-rich deep waters back to the sunlit surface layer, sustaining global ocean productivity. The "biological pump" maintains this vertical gradient in nutrients through uptake, vertical transport, and remineralization of organic matter, storing carbon in the deep ocean that is isolated from the atmosphere on centennial and millennial timescales, lowering atmospheric CO_2 levels by hundreds of microatmospheres (Sarmiento & Toggweiler, 1984; Knox & McElroy, 1984; Volk & Hoffert, 1985; Ito et al., 2005). The biological pump resists simple mechanistic characterization due to the complex suite of biological, chemical, and physical processes involved (Boyd et al., 2019), so the fate of exported organic carbon is typically described using a depth-dependent profile to evaluate the degradation of sinking particulate matter.

Various remineralization profiles can be derived from assumptions about particle degradability and sinking speed(s) (Suess, 1980; Martin et al., 1987; Middelburg, 1989;

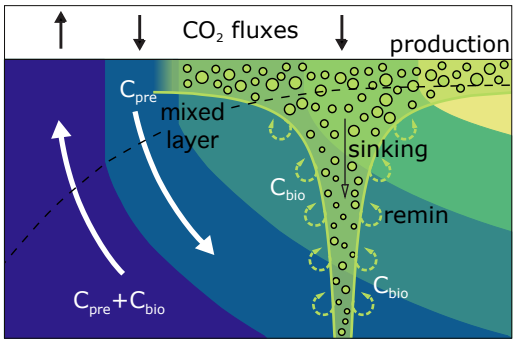

Figure 1. Schematic of the biological pump. Primary production by phytoplankton takes up carbon and nutrients in the sunlit surface ocean creating a pool of sinking particulate organic matter. Unused carbon and nutrients are subducted from the surface and conservatively transported into the ocean interior (the "preformed" carbon concentration, C_{pre}). Exported and sinking particles are remineralized at depth returning the organic matter to its inorganic constituents that are accumulated by watermasses (as the "biological" carbon concentration, C_{bio}). Upwelling from the deep ocean returns both preformed and remineralized carbon and nutrients to the surface mixed layer.

Banse, 1990; Armstrong et al., 2001; Lutz et al., 2002; Rothman & Forney, 2007; Kriest & Oschlies, 2008; Cael & Bisson, 2018). The ubiquitous "Martin Curve" (Martin et al., 1987) is a power-law profile (Eq. 1) that assumes slower-sinking and/or more labile organic matter is preferentially depleted near the surface causing increasing sinking speed and/or remineralization timescale with depth (Fig. 2a).

$$f_p(z) = C_p z^{-b}, \tag{1}$$

where $f_p(z)$ (moles per square meter per second) representing a fraction of particulate flux at depth z (meters), C_p (per meter) corresponds[1] to the initial flux from the productive layer near the surface (Buesseler et al., 2020), and b is a nondimensional parameter controlling how f_p decreases with depth.

Considerable effort has been dedicated to determining value(s) for the exponent, b (e.g., Martin et al., 1987, 1993; Berelson, 2001; Primeau, 2006; Honjo et al., 2008; Henson et al., 2012; Gloege et al., 2017; Wilson et al., 2019). Open ocean particulate flux observations from the North Pacific (Martin et al., 1987) indicate a b value of 0.858. Fur-

[1] Eq. 1 is often normalized to a reference depth z_o but this parameter is readily absorbed into C_p.

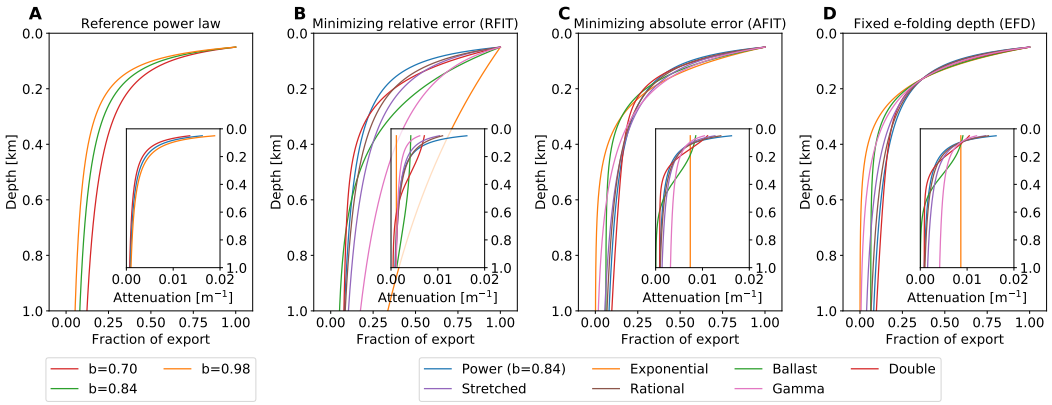

Figure 2. Fraction of sinking particulate organic matter exported from the 50 m surface layer remaining at each depth for (a) the reference power-law (Eq. 1) with exponents 0.84 ± 0.14, and six alternative functions (Eq. S1–S6) fit to the reference power-law curve ($b = 0.84$) by (b) statistically minimizing the relative error ("RFIT"), or (c) the absolute error ("AFIT"), and (d) matching the e-folding depth scale of 164 m ("EFD"). See Materials and Methods, Table S1 for fitting details, coefficients, and fit statistics. Inset plots show the attenuation rate of the export flux with depth $\left[\frac{1}{f}\frac{\partial f}{\partial z}, m^{-1}\right]$.

ther analyses of expanded sediment trap datasets suggest a possible range of approximately 0.84 ± 0.14 for the global b value (Martin et al., 1993; Berelson, 2001; Primeau, 2006; Honjo et al., 2008; Gloege et al., 2017), though a much wider range has been observed when including regional variability in b and optically- and geochemically-derived flux estimates (Henson et al., 2012; Guidi et al., 2015; Pavia et al., 2019). This may result from differences in temperature (Matsumoto, 2007), microbial community composition (Boyd & Newton, 1999), particle composition (Armstrong et al., 2001), oxygen concentration (Devol & Hartnett, 2001), or external factors such as mineral ballasting (Pabortsava et al., 2017).

Uncertainty in the value of b translates to uncertainty in the biological pump's impact on the ocean carbon sink, atmosphere-ocean carbon partitioning, and climate model projections. Thus, constraining b for the modern ocean and how it may differ in the past, or the future, is of much interest from a climate perspective, with one estimate placing an economic value of $0.5 trillion USD on reducing these uncertainties (Jin et al., 2020). Varying a global value of b between 0.50–1.4 altered atmospheric pCO_2 by 86–185 μatm in an influential modeling study (Kwon et al., 2009): Higher values of b result in enhanced

particle remineralization at shallower depths. Shallow watermasses are more frequently ventilated, allowing remineralized CO_2 to be released back into the atmosphere on shorter timescales. Due to this depth-dependence, a small change of degradation depth can appreciably change atmospheric pCO_2 (Yamanaka & Tajika, 1996; Kwon et al., 2009). Varying b over the plausible range in global values between 0.70–0.98 produces a more modest change in atmospheric pCO_2, over the range of (-16,+12)μatm (Gloege et al., 2017), while the modeled uncertainty in atmospheric pCO_2 associated with regional variation in b is estimated between 5–15 μatm (Wilson et al., 2019).

Biogeochemical models are subject not only to parametric uncertainty (which value for b and how b varies in space and time), but also structural uncertainty, i.e. which equation(s) to choose for the vertical flux of organic matter. The Martin Curve power-law is an empirical fit to sediment trap data, but several other functional forms have also been put forward (Suess, 1980; Middelburg, 1989; Banse, 1990; Armstrong et al., 2001; Lutz et al., 2002; Dutkiewicz et al., 2005; Rothman & Forney, 2007; Marsay et al., 2015) that fit sediment trap fluxes equivalently well and have equal if not better mechanistic justification (Cael & Bisson, 2018). Atmospheric pCO_2 and many other global biogeochemical properties will be affected by this structural uncertainty, so it is critical to evaluate the impact of choosing one remineralization profile "shape" over another.

We assess the effect of remineralization profile shape on biological pump strength and evaluate a comprehensive estimate of structural uncertainty in terms of atmosphere-ocean carbon partitioning in a global ocean biogeochemistry model. We substitute the reference power-law curve for six different remineralization profiles (exponential (Banse, 1990; Dutkiewicz et al., 2005; Marsay et al., 2015; Gloege et al., 2017), ballast (Armstrong et al., 2001; Gloege et al., 2017), double exponential (Lutz et al., 2002), stretched exponential (Middelburg, 1989; Cael & Bisson, 2018), rational (Suess, 1980), and gamma (Rothman & Forney, 2007) functions[2]), each corresponding to a basic mechanistic description of particle flux (Cael & Bisson, 2018), that are constrained to the reference profile by statistically minimizing misfits or by matching degradation depth scales (Kwon et al., 2009). These simulations indicate that structural uncertainty is an appreciable component, around one third, of total uncertainty for understanding the biological pump: changing remineralization functional form alters atmospheric pCO_2 by ∼10-15 μatm de-

[2] See Supporting Information for derivations of these profiles

pending on how structural uncertainty is quantified, equivalent to ∼0.08 uncertainty in a global value of the power-law exponent, b, and similar to the uncertainty resulting from regional variation of b.

Our results underscore the importance of characterizing basic mechanisms governing the biological pump. Furthermore, our results corroborate that depth-dependence of these mechanisms is particularly important (Gehlen et al., 2006; Kriest & Oschlies, 2008): not only is biological pump-driven carbon storage an important control on atmospheric pCO_2, but we find that particle degradation in the upper ocean must also decrease rapidly for a sufficient quantity of carbon to become isolated in the deep ocean. While a given flux curve may be chosen for historical reasons or mathematical convenience, its skill should be compared to those of other idealized flux profile parameterizations in Earth System Models used for projections of future climate.

2 Materials and Methods

2.1 Fitting the alternative remineralization curves.

We fit the alternative functions for export fluxes and remineralization (Fig. 2, Eq. S1–S6, see Supporting Information) to the reference power-law curve (Eq. 1) with the exponent $b = 0.84$ using nonlinear regression on the native model grid interfaces to minimize the absolute curve mismatch ("ABS" simulations). Points were weighted equally, except for the heavily weighted top level to ensure all the profiles pass through the same value as the control profile (i.e. fraction of export from the surface layer is 1.0). We further matched the e-folding depth of remineralization to the reference ("EFD" simulations) by adding a second heavily weighted point to the reference power-law at 164 m depth ($z_0 e^{(1/b)}$), with an export fraction of e^{-1}. In a third set ("RFIT" simulations), the nonlinear regression is performed in log-space to minimize the relative error the reference profile match. Goodness of fit is evaluated by the Standard Error of Regression, $\mathcal{S}$, which is the sum of squared residuals, divided by statistical degrees of freedom (number of points minus number of parameters). Coefficients and $\mathcal{S}$ values for the eighteen curves are given in Table S1.

2.2 Numerical ocean biogeochemistry model.

Alternative remineralization profiles are substituted into global ocean simulations of a coarse resolution (3°, 15 vertical level) global configuration of the Massachusetts Institute of Technology general circulation model, MITgcm (Marshall et al., 1997), coupled to an idealized ocean biogeochemistry model (Najjar et al., 2007; Dutkiewicz et al., 2006; Parekh et al., 2006) that captures the magnitude and variation of observed air-sea fluxes of CO_2 (Lauderdale et al., 2016), and has been widely used in theoretical carbon cycle studies (Parekh et al., 2006; Dutkiewicz et al., 2006; Goodwin et al., 2007; Najjar et al., 2007; Lauderdale et al., 2013, 2017).

Two-thirds of surface production (which depends on light, nutrients, and iron) is channelled into dissolved organic matter that is remineralized with a timescale of 6 months (Yamanaka & Tajika, 1997), while one-third is exported via sinking particulate organic matter subject to depth-dependent remineralization rates. Elemental biological transformations are related using fixed stoichiometric ratios $R_{C:N:P:Fe:O_2}$ = 117:16:1:4.68×10^{-4}:-170 (Anderson & Sarmiento, 1994). The total ocean-atmosphere carbon inventory is conserved as there is no riverine carbon input or sediment carbon burial. Our model includes tracers to separate the *in situ* concentrations of carbon (Fig. 1) into: (i) a component subducted from the surface layer and transported conservatively by ocean circulation (the "preformed" carbon concentration, C_{pre}), and (ii) a component that integrates export and remineralization of organic matter as a watermass transits the ocean interior (the "biological" carbon concentration, C_{bio}), connecting more directly to the biological pump (Ito & Follows, 2005). We integrate simulations for 10,000 years toward steady state in atmosphere-ocean carbon partitioning.

3 Results

3.1 Varying the exponent of the reference power-law curve.

Global power-law exponent, b, estimates range from 0.70 (Primeau, 2006) based on sediment traps to 0.97 based on inverse models fit to tracer distributions (Kwon & Primeau, 2008; Kwon et al., 2009). These values match the global b interquartile range of 0.70–0.98 in (Gloege et al., 2017). We integrate three simulations with $b = 0.84 \pm 0.14$ (Fig. 2a) using the standard power-law parameterization (Eq. 1) to produce a base-

line estimate of biological pump parametric uncertainty. The reference simulation has the exponent $b = 0.84$.

Higher b values cause the fraction of sinking particulate matter to decrease faster with depth, that is, attenuation ($1/f_p \cdot \partial f_p/\partial z$) is higher in the upper ocean, whereas lower exponents have less attenuation and a larger proportion of export reaching the deep ocean (Figs. 2a and S1a–f). A negative feedback occurs near the surface in our simulations. For example, when b is increased, higher rates of upper ocean attenuation cause an increase in surface nutrient availability, and therefore more overall biological production (see ΔB_C, Table S2). Local biological activity enhancement increases local rates of particle export, evaluated by integrated fluxes through the deepest mixed layer depth (ΔE_{mld}, Table S2). However, higher shallow export is compensated by greater upper ocean remineralization, due to larger exponent value, resulting instead in reduced export flux anomalies through 1 km depth (ΔE_{1km}, Table S2), and vice versa when b is decreased. The global ocean reservoir of biological carbon changes proportionally with ΔE_{1km} (Figs. 3, blue symbols, S1g–i, and ΔC_{bio}, Table S2) and inversely-proportional to ΔE_{mld} (Fig. S4a).

3.2 Impact of alternative remineralization curve shape.

Six alternative remineralization profiles, obtained from simplifying assumptions about the balance between particles' vertical transport and degradation (Eq. S1–S6), are characterized by objectively evaluating parameters to match the reference power-law curve ($b = 0.84$) as closely as possible (Fig. 2b–d, Table S1): In two groups of simulations, parameters are found by statistically minimizing the relative error ("RFIT") or the absolute error ("AFIT") of the nonlinear fit of each curve to the reference profile. In a third group of simulations, parameters are found that match the reference curve's 164 m e-folding depth of remineralization ("EFD", the depth at which the flux has been attenuated to a factor of $1/e$).

The simple exponential and gamma function fits are poorer than the other functions (Fig. 2b–d) because these profiles cannot capture a strong depth-change in remineralization. Simulations with lower-attenuation profiles result in increased export fluxes through the 1 km depth horizon (ΔE_{1km}), and vice versa, as with the simulations varying b (Fig. 3). These particulate flux anomalies translate into changes in the distribution of biological carbon (C_{bio}), with positive export flux anomalies corresponding to in-

crease in the biological carbon pool (Fig. 3), while negative export flux anomalies result in lower biological carbon concentrations (Fig. S3). For instance, in RFIT simulations, the exponential and gamma profiles show an increase in 1 km export fluxes and biological carbon storage, while the reverse occurs for exponential and gamma profiles in AFIT and EFD simulations. The ballast profile has a more complex distribution of biological carbon anomalies in surface, intermediate, and deep waters (Fig. S3) such that the relationship between export flux and ΔC_{bio} is better captured by considering deeper horizons (e.g. 2 km, Fig. S4b).

3.3 Evaluating structural uncertainty of the biological pump.

Altering the strength of the biological pump leads to changes in air-sea carbon balance. The reference simulation has a steady-state atmospheric pCO_2 of 269.3 μatm. Increasing b from 0.70 to 0.98 increases pCO_2 by 46.36 μatm in this model (range: -21.6–24.8 μatm, wide grey bars in Fig. 4, Table S2). This is higher than the "nutrient restoring" case in (Kwon et al., 2009), but lower than their "constant export" case, consistent with our model's dynamic biological productivity response.

Alternative profiles with reduced export flux through 1 km and reduced biological carbon storage result in increased atmospheric pCO_2, and vice versa (Fig. 4, Table S3). The double exponential function has the most free parameters (four) and therefore fits the power-law extremely well, producing small differences in atmospheric pCO_2 (less than 2 μatm). The rational function also agrees well, but could produce larger anomalies if the reference profile's b-value was further from 1.0, i.e. 0.70. Stretched exponential and ballast curves produce moderate changes in atmospheric pCO_2 but are generally smaller than, or similar to, the 0.14 changes in b for the power-law curves (Fig. 4). However, the simple exponential and gamma anomalies clearly deviate from the other simulations, with greater biological carbon concentrations and drawdown of atmospheric CO_2 for the RFIT simulations, and the inverse for AFIT and EFD simulations. Export fluxes and remineralization are significantly different in the upper ocean for these parameterizations, which can be explained by their small dynamic range in attenuation (Fig. 2 insets): simple exponential and gamma parameterizations cannot have both short remineralization lengthscales in the upper ocean and long remineralization lengthscales in the deep ocean.

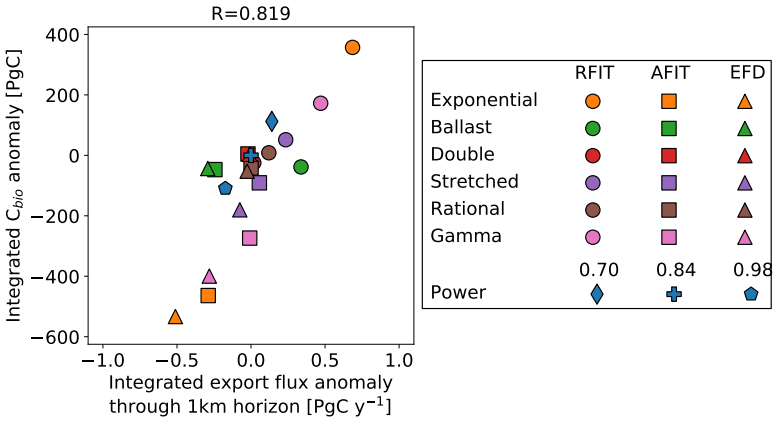

Figure 3. Change in the integrated export flux rate [PgC y^{-1}] passing through the 1 km depth level against integrated biological carbon reservoir anomaly [PgC], both with respect to the power-law curve where b=0.84 (Martin et al., 1987). Three power-law simulations (b=0.84±0.14) are indicated by the blue symbols (diamond, cross, and pentagon), circle, square, and triangle symbols indicate that profile coefficients (Eq. S1–S6) were derived by minimizing the relative fit error ("RFIT"), minimizing the absolute fit error ("AFIT"), and fixing the e-folding depth of remineralization ("EFD") to the reference power-law curve. Values are given in Tables S2 and S3.

There are multiple ways to compare parametric and structural uncertainty quantitatively. Parametric uncertainty is found by varying the power-law exponent within its plausible global range ($b = 0.84 \pm 0.14$), producing atmospheric pCO_2 anomalies of 21.6–24.8 μatm (Fig. 4, Table S3). For structural uncertainty, the median change in absolute atmospheric pCO_2 is 12.47±10.67 μatm (b-anomaly equivalent of 0.07±0.06) across all simulations with alternate functional forms[3]. For RFIT, AFIT, and EFD simulations separately, the medians are 15.15±10.40, 10.65±7.30, and 20.57±15.37 μatm, respectively, giving a 15.15±4.51 μatm grand median (b-anomaly equivalent of 0.09±0.03). Excluding profiles with small dynamic ranges in attenuation, the overall medians for RFIT, AFIT, and EFD are 10.07±2.32, 7.96±2.69, and 10.57±1.98 μatm, respectively, with a 10.07±0.50 μatm grand median (b-anomaly equivalent of 0.06±0.00). In summary, our results are largely robust, indicating a structural uncertainty of 10–15 μatm, roughly half of parametric un-

[3] We choose the median±median absolute deviation so that our result is robust to large anomalies associated with simple exponential and gamma functional forms.

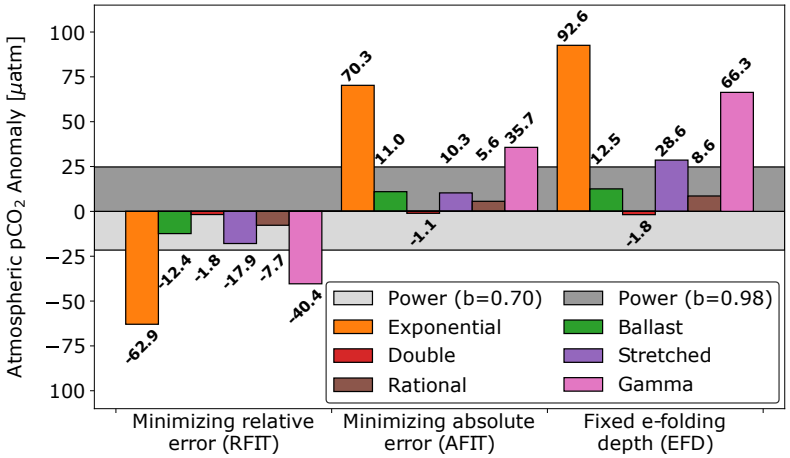

Figure 4. Atmospheric pCO_2 anomalies (μatm) of different remineralization profiles with respect to the reference power-law ($b = 0.84$) for power-law exponent values $b = 0.70$ and 0.98, and statistical fits of alternative profiles minimizing relative error ("RFIT", left), minimizing absolute error ("AFIT", middle), and matching the 164 m e-folding depth ("EFD", right) of the reference curve.

certainty for the biological pump (22–25 μatm, $b = 0.84 \pm 0.14$), analogous to a $\sim$0.08 change in b.

3.4 Role of nonlinearity in the biological pump.

Our simulations also allow us to tease apart two fundamental aspects of the biological pump: In terms of atmospheric CO_2 influence, (i) how much is due to ocean biological carbon storage, and (ii) how much is due to the shape of remineralization profile?

A simulation "NOPOM" represents a hypothetical ocean with no particulate organic matter export and without a biological carbon pool. Instead, biological production is channelled into semi-labile dissolved organic matter that is remineralized near the surface. Atmospheric pCO_2 in NOPOM increases 165.4 μatm (Table S2) with respect to the reference power-law.

Compared to NOPOM, the simple exponential simulations in AFIT and EFD have significant 1 km export fluxes and large stores of biological carbon (Table S3). That is, they have a substantial biological pump, but atmospheric pCO_2 is only 95.1 and 72.8 μatm

lower than NOPOM, respectively. Thus, only about half of the biological pump's influence on atmosphere-ocean carbon partitioning (∼80 μatm) can be attributed to export of particulate organic matter and biological carbon storage (Fig. S5).

Now, comparing AFIT/EFD exponential profiles to the reference power-law (or indeed any high dynamic-range curves), there are only modest differences in 1 km export fluxes and biological carbon storage. Nevertheless, AFIT/EFD exponential profile 2 km export fluxes remain closer to NOPOM than the other curves (Table S3). Thus, we can attribute the remaining ∼80 μatm atmospheric pCO_2 anomaly to the effect of decreasing remineralization with depth (Fig. 2c–d insets), since attenuation is constant for the simple exponential profiles, but varies with the other curves.

In other words, increasing remineralization lengthscale with depth appears to be as important for air-sea carbon partitioning as export and storage of biological carbon (Fig. S5).

4 Discussion and Conclusions

Atmospheric CO_2 levels are intimately tied to the strength of the ocean's biological pump, comprising linked processes of primary production, export of organic matter from the upper ocean, and the degradation of particles back to inorganic constituents with depth. The challenge of measuring particulate fluxes via sediment traps, optical proxies, or geochemical methods (Martin et al., 1987; Berelson, 2001; Honjo et al., 2008; Henson et al., 2012; Guidi et al., 2015; Pavia et al., 2019), the spatiotemporal variability of fluxes, and the complexity of the mechanisms governing them all introduce uncertainty into representation of the biological pump in ocean biogeochemistry, ecosystem, and climate models. We explored the impact of structural uncertainty—remineralization profile shape—on atmosphere-ocean carbon partitioning, using seven mechanistically-distinct functional forms of particulate organic matter flux that capture observational spread equivalently well (Cael & Bisson, 2018). Steady-state atmospheric pCO_2 is inversely related to the biological carbon pool, thus profiles with more efficient export through 1 km, and greater biological carbon storage, lead to atmospheric CO_2 drawdown.

In our model, a 0.14 change in the power-law exponent, b, results in a 22–25 μatm change in atmospheric pCO_2, indicating that structural uncertainty revealed by our simulations of 10–15 μatm is equivalent to ∼0.08 change in the global b value. Thus struc-

tural uncertainty is roughly half that of parameteric uncertainty, a substantial portion, one third, of total uncertainty in understanding the biological pump. In addition our result is in the upper range of the 5-15 μatm uncertainty associated with regional variation in b (Wilson et al., 2019).

Historically, the focus been on remineralization length*scale* (Kwon et al., 2009), but our results imply that multiple length*scales* of attenuation are critical to the biological pump's global impact, indicating that vertical gradient in attenuation is a first-order control on climate. The simple exponential functional form, with constant depth attenuation, results in much larger atmospheric pCO_2 anomalies of $\sim$80μatm for AFIT and EFD simulations, despite being statistically fit to be as similar to the reference power law as possible (and similarly for gamma function profiles). This is roughly half the $\sim$165μatm increase that results from removing the biological pump altogether (NOPOM), highlighting the importance for the air-sea carbon balance, not only of the existence of a biological pump that maintains interior ocean biological carbon stores, but also its non-linearity (Fig. S5). More specifically, significant decrease of attenuation with depth is a key factor in the biological pump's modulation of atmospheric CO_2 levels. Even when the exponential profiles' parameters are determined by matching the e-folding remineralization depth of the reference power-law curve (Kwon et al., 2009), the result is still large atmospheric pCO_2 anomalies caused by small dynamic range in attenuation.

Our study is the first to evaluate structural uncertainty in the ocean's biological pump. Although previous studies have compared individual, or a subset, of the alternative remineralization curves used here (e.g., Yamanaka & Tajika, 1996; Gehlen et al., 2006; Kriest & Oschlies, 2008; Gloege et al., 2017) with a focus on minimizing model-observational differences, none has attempted to evaluate this structural uncertainty, which we do here by comparing six alternative functional forms fit to a reference power-law profile.

As Earth System Models continue to rely on simple biological pump parameterizations, our estimate of structural uncertainty underscores the importance of research aimed at improving the basic mechanistic characterization of the biological pump (Boyd et al., 2019), and particularly the depth-dependence or evolution of these mechanisms. A better process-based understanding is critical to choosing between these parameterizations based on their mechanistic underpinnings and thus reducing structural uncer-

tainty, because empirical fits to flux measurements alone cannot currently do so (Cael & Bisson, 2018). This is even more the case for modeling past climate or projections of future change. In our simulations, the parameterizations were forced to be as similar as possible, but functional forms based on different processes will have different sensitivities to temperature and other phenomena, and therefore will produce divergent projections and different climate feedbacks. It would therefore be valuable to compare these different functional forms within state-of-the-art Earth System Models to improve confidence in projections involving biosphere-climate interactions.

Acknowledgments

We thank Lauren Hinkel (MIT) for copyediting and clarity advice on previous drafts of this manuscript. **Funding:** JML was supported by the US National Science Foundation ("Dust PIRE", 1545859); BBC was supported by a Simons Postdoctoral Fellowship in Marine Microbial Ecology, the UK National Environmental Research Council (NE/R015953/1), and the EU H2020 project COMFORT (820989). This work reflects only the authors' views; the European Commission and their executive agency are not responsible for any use that may be made of the information the work contains. **Author contributions:** JML and BBC contributed equally to the design, analysis, interpretation, and write up of this manuscript. **Competing interests:** The authors declare no competing interests. **Data availability:** Preliminary model input, code, and output processing routines can be accessed via GitHub (*https://github.com/seamanticscience/Lauderdale_and_Cael_Exports*, to be updated and uploaded to *Zenodo.org* open science archive).

References

Anderson, L. A., & Sarmiento, J. L. (1994). Redfield ratios of remineralization determined by nutrient data analysis. *Global Biogeochem. Cycles*, *8*, 65–80.

Armstrong, R. A., Lee, C., Hedges, J. I., Honjo, S., & Wakeham, S. G. (2001). A new, mechanistic model for organic carbon fluxes in the ocean based on the quantitative association of poc with ballast minerals. *Deep Sea Res. Part II*, *49*(1), 219–236. doi: 10.1016/S0967-0645(01)00101-1

Banse, K. (1990). New views on the degradation and disposition of organic particles as collected by sediment traps in the open sea. *Deep Sea Research Part A. Oceanographic Research Papers*, *37*(7), 1177–1195. doi: 10.1016/0198-0149(90)

90058-4

Berelson, W. M. (2001). The flux of particulate organic carbon into the ocean interior: A comparison of four U.S. JGOFS regional studies. *Oceanography*, *14*, 59–67. doi: 10.5670/oceanog.2001.07

Boyd, P. W., Claustre, H., Levy, M., Siegel, D. A., & Weber, T. (2019). Multi-faceted particle pumps drive carbon sequestration in the ocean. *Nature*, *568*(7752), 327–335. doi: 10.1038/s41586-019-1098-2

Boyd, P. W., & Newton, P. P. (1999). Does planktonic community structure determine downward particulate organic carbon flux in different oceanic provinces? *Deep Sea Res. Part I*, *46*(1), 63–91. doi: 10.1016/S0967-0637(98)00066-1

Buesseler, K. O., Boyd, P. W., Black, E. E., & Siegel, D. A. (2020). Metrics that matter for assessing the ocean biological carbon pump. *Proc. Nat. Acad. Sci.*, *117*(18), 9679. doi: 10.1073/pnas.1918114117

Cael, B. B., & Bisson, K. (2018). Particle flux parameterizations: Quantitative and mechanistic similarities and differences. *Front. Mar. Sci.*, *5*, 395. doi: 10.3389/fmars.2018.00395

Devol, A. H., & Hartnett, H. E. (2001). Role of the oxygen-deficient zone in transfer of organic carbon to the deep ocean. *Limnol. Oceanogr.*, *46*(7), 1684–1690. doi: 10.4319/lo.2001.46.7.1684

Dutkiewicz, S., Follows, M. J., Heimbach, P., & Marshall, J. (2006). Controls on ocean productvity and air–sea carbon flux: An adjoint model sensitivity study. *Geophys. Res. Lett.*, *33*. doi: 10.1029/2005GL024987

Dutkiewicz, S., Follows, M. J., & Parekh, P. (2005). Interactions of the iron and phosphorus cycles: A three dimensional model study. *Global Biogeochem. Cycles*, *19*. doi: 10.1029/2004GB002342

Gehlen, M., Bopp, L., Emprin, N., Aumont, O., Heinze, C., & Ragueneau, O. (2006). Reconciling surface ocean productivity, export fluxes and sediment composition in a global biogeochemical ocean model. *Biogeosciences*, *3*(4), 521–537. doi: 10.5194/bg-3-521-2006

Gloege, L., McKinley, G. A., Mouw, C. B., & Ciochetto, A. B. (2017). Global evaluation of particulate organic carbon flux parameterizations and implications for atmospheric pCO_2. *Global Biogeochem. Cycles*, *31*(7), 1192–1215. doi: 10.1002/2016GB005535

Goodwin, P., Williams, R. G., Follows, M. J., & Dutkiewicz, S. (2007). Ocean-atmosphere partitioning of anthropogenic carbon dioxide on centennial timescales. *Global Biogeochem. Cycles*, *21*(1), GB1014. doi: 10.1029/2006GB002810

Guidi, L., Legendre, L., Reygondeau, G., Uitz, J., Stemmann, L., & Henson, S. A. (2015). A new look at ocean carbon remineralization for estimating deep-water sequestration. *Global Biogeochem. Cycles*, *29*(7), 1044–1059. doi: 10.1002/2014GB005063

Henson, S. A., Sanders, R., & Madsen, E. (2012). Global patterns in efficiency of particulate organic carbon export and transfer to the deep ocean. *Global Biogeochem. Cycles*, *26*(1). doi: 10.1029/2011GB004099

Honjo, S., Manganini, S. J., Krishfield, R. A., & Francois, R. (2008). Particulate organic carbon fluxes to the ocean interior and factors controlling the biological pump: A synthesis of global sediment trap programs since 1983. *Prog. Oceanogr.*, *76*(3), 217–285. doi: 10.1016/j.pocean.2007.11.003

Ito, T., & Follows, M. J. (2005). Preformed phosphate, soft tissue pump and atmospheric CO_2. *J. Mar. Res.*, *63*, 813–839.

Ito, T., Parekh, P., Dutkiewicz, S., & Follows, M. J. (2005). The Antarctic circumpolar productivity belt. *Geophys. Res. Lett.*, *32*. doi: 10.11029/2005GL023021

Jin, D., Hoagland, P., & Buesseler, K. O. (2020). The value of scientific research on the ocean's biological carbon pump. *Science of The Total Environment*, *749*, 141357. doi: 10.1016/j.scitotenv.2020.141357

Knox, F., & McElroy, M. B. (1984). Changes in atmospheric CO_2: Influence of the marine biota at high latitude. *J. Geophys. Res.*, *89*(3), 4629–4637.

Kriest, I., & Oschlies, A. (2008). On the treatment of particulate organic matter sinking in large-scale models of marine biogeochemical cycles. *Biogeosciences*, *5*(1), 55–72. doi: 10.5194/bg-5-55-2008

Kwon, E. Y., & Primeau, F. (2008). Optimization and sensitivity of a global biogeochemistry ocean model using combined in situ DIC, alkalinity, and phosphate data. *J. Geophys. Res.*, *113*(C8). doi: 10.1029/2007JC004520

Kwon, E. Y., Primeau, F., & Sarmiento, J. L. (2009). The impact of remineralization depth on the air–sea carbon balance. *Nature Geosci.*, *2*(9), 630–635. doi:

10.1038/ngeo612

Lauderdale, J. M., Dutkiewicz, S., Williams, R. G., & Follows, M. J. (2016). Quantifying the drivers of ocean-atmosphere CO_2 fluxes. *Global Biogeochem. Cycles*, *30*(7), 983–999. doi: 10.1002/2016GB005400

Lauderdale, J. M., Naveira Garabato, A. C., Oliver, K. I. C., Follows, M. J., & Williams, R. G. (2013). Wind-driven changes in Southern Ocean residual circulation, ocean carbon reservoirs and atmospheric CO_2. *Climate Dynam.*, *41*(7), 2145–2164. doi: 10.1007/s00382-012-1650-3

Lauderdale, J. M., Williams, R. G., Munday, D. R., & Marshall, D. P. (2017). The impact of southern ocean residual upwelling on atmospheric CO_2 on centennial and millennial timescales. *Climate Dynam.*, *48*(5), 1611–1631. doi: 10.1007/s00382-016-3163-y

Lutz, M., Dunbar, R., & Caldeira, K. (2002). Regional variability in the vertical flux of particulate organic carbon in the ocean interior. *Global Biogeochem. Cycles*, *16*(3), 11-1–11-18. doi: 10.1029/2000GB001383

Marsay, C. M., Sanders, R. J., Henson, S. A., Pabortsava, K., Achterberg, E. P., & Lampitt, R. S. (2015). Attenuation of sinking particulate organic carbon flux through the mesopelagic ocean. *Proc. Nat. Acad. Sci.*, *112*(4), 1089. doi: 10.1073/pnas.1415311112

Marshall, J., Adcroft, A., Hill, C., Perelman, L., & Heisey, C. (1997). A finite-volume, incompressible Navier Stokes model for studies of the ocean on parallel computers. *J. Geophys. Res.*, *102*(C3), 5753–5766.

Martin, J. H., Fitzwater, S. E., Michael Gordon, R., Hunter, C. N., & Tanner, S. J. (1993). Iron, primary production and carbon-nitrogen flux studies during the jgofs north atlantic bloom experiment. *Deep Sea Res. Part II*, *40*(1), 115–134. doi: 10.1016/0967-0645(93)90009-C

Martin, J. H., Knauer, G. A., Karl, D. M., & Broenkow, W. W. (1987). Vertex: carbon cycling in the northeast pacific. *Deep-Sea Res.*, *34*(267–285).

Matsumoto, K. (2007). Biology-mediated temperature control on atmospheric pCO_2 and ocean biogeochemistry. *Geophys. Res. Lett.*, *34*(20). doi: 10.1029/2007GL031301

Middelburg, J. J. (1989). A simple rate model for organic matter decomposition in marine sediments. *Geochim. Cosmochim. Acta*, *53*(7), 1577–1581. doi: 10

458 .1016/0016-7037(89)90239-1

459 Najjar, R. G., Jin, X., Louanchi, F., Aumont, O., Caldeira, K., Doney, S. C., ...
460 Yool, A. (2007). Impact of circulation on export production, dissolved organic
461 matter, and dissolved oxygen in the ocean: Results from phase ii of the ocean
462 carbon-cycle model intercomparison project (ocmip-2). *Global Biogeochem.*
463 *Cycles*, *21*(3). doi: 10.1029/2006GB002857

464 Pabortsava, K., Lampitt, R. S., Benson, J., Crowe, C., McLachlan, R., Le Moigne,
465 F. A. C., ... Woodward, E. M. S. (2017). Carbon sequestration in the deep
466 atlantic enhanced by saharan dust. *Nature Geosci.*, *10*(3), 189–194. doi:
467 10.1038/ngeo2899

468 Parekh, P., Follows, M. J., Dutkiewicz, S., & Ito, T. (2006). Physical and biological
469 regulation of the soft tissue carbon pump. *Paleoceanography*, *21*. doi: 10.1026/
470 2005PA001258

471 Pavia, F. J., Anderson, R. F., Lam, P. J., Cael, B. B., Vivancos, S. M., Fleisher,
472 M. Q., ... Edwards, R. L. (2019). Shallow particulate organic carbon regen-
473 eration in the south pacific ocean. *Proc. Nat. Acad. Sci.*, *116*(20), 9753. doi:
474 10.1073/pnas.1901863116

475 Primeau, F. (2006). On the variability of the exponent in the power law depth
476 dependence of poc flux estimated from sediment traps. *Deep Sea Res. Part I*,
477 *53*(8), 1335–1343. doi: 10.1016/j.dsr.2006.06.003

478 Rothman, D. H., & Forney, D. C. (2007). Physical model for the decay and preserva-
479 tion of marine organic carbon. *Science*, *316*(5829), 1325. doi: 10.1126/science
480 .1138211

481 Sarmiento, J. L., & Toggweiler, J. R. (1984). A new model for the role of the oceans
482 in determining atmospheric pCO_2. *Nature*, *308*, 621–624.

483 Suess, E. (1980). Particulate organic carbon flux in the oceans—surface productivity
484 and oxygen utilization. *Nature*, *288*(5788), 260–263. doi: 10.1038/288260a0

485 Volk, T., & Hoffert, M. I. (1985). Ocean carbon pumps: Analysis of relative
486 strengths and efficiencies in ocean-driven atmospheric CO_2 changes. In
487 T. E. Sundquist & W. S. Broecker (Eds.), *The carbon cycle and atmospheric*
488 *CO_2: Natural variations Archean to present.* (Vol. 32, pp. 99–110). American
489 Geophysical Union, Washington, D. C.

490 Wilson, J. D., Barker, S., Edwards, N. R., Holden, P. B., & Ridgwell, A. (2019).

Sensitivity of atmospheric CO_2 to regional variability in particulate organic matter remineralization depths. *Biogeosciences*, *16*(14), 2923–2936. doi: 10.5194/bg-16-2923-2019

Yamanaka, Y., & Tajika, E. (1996). The role of the vertical fluxes of particulate organic matter and calcite in the oceanic carbon cycle: Studies using an ocean biogeochemical general circulation model. *Global Biogeochem. Cycles*, *10*(2), 361–382. doi: 10.1029/96GB00634

Yamanaka, Y., & Tajika, E. (1997). Role of dissolved organic matter in the marine biogeochemical cycle: Studies using an ocean biogeochemical general circulation model. *Global Biogeochem. Cycles*, *11*(4), 599–612.

Figure 1.

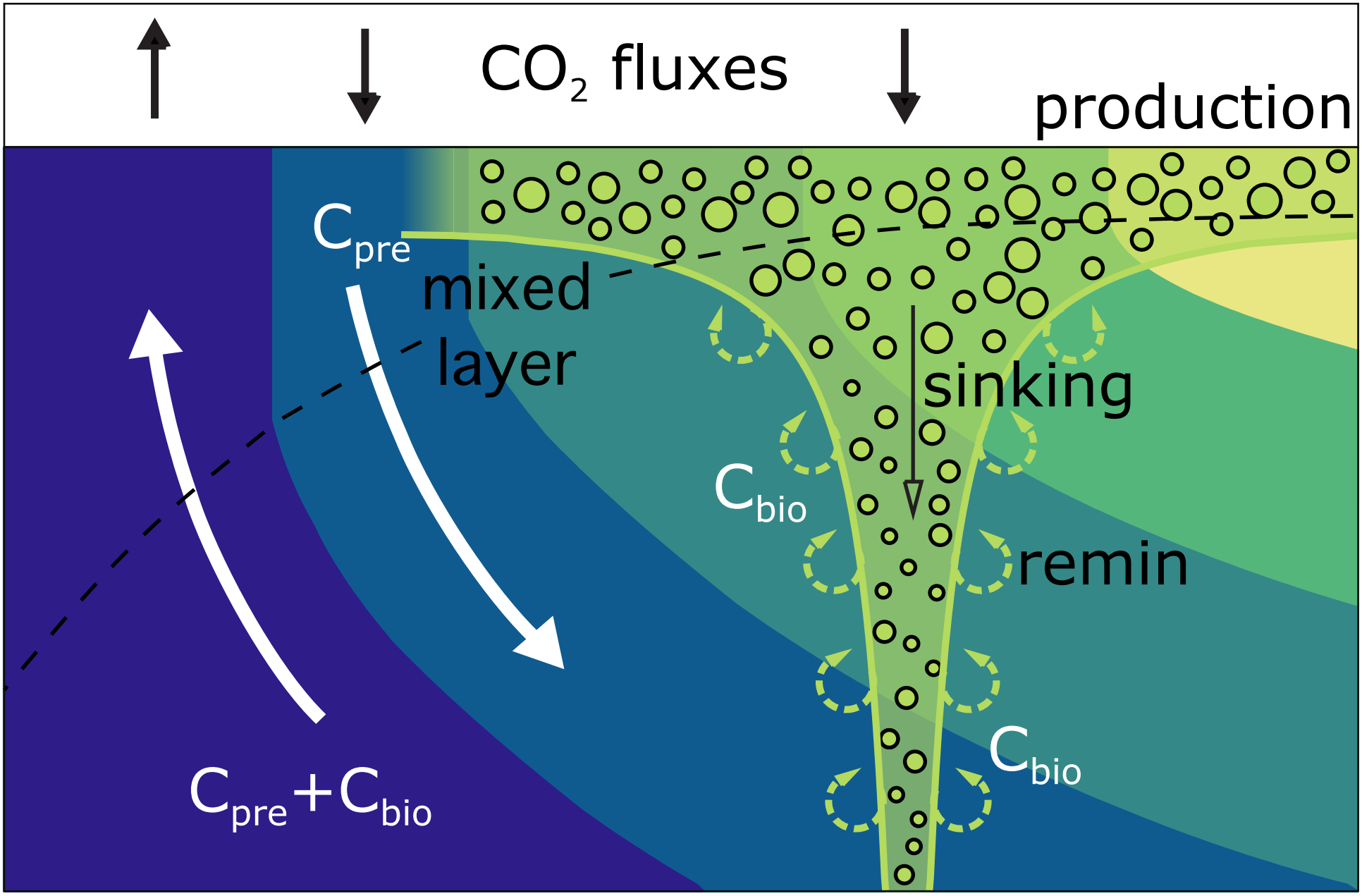
CO_2 fluxes
production
C_{pre}
mixed
layer
sinking
C_{bio}
remin
C_{bio}
$C_{pre}+C_{bio}$

Figure 2.

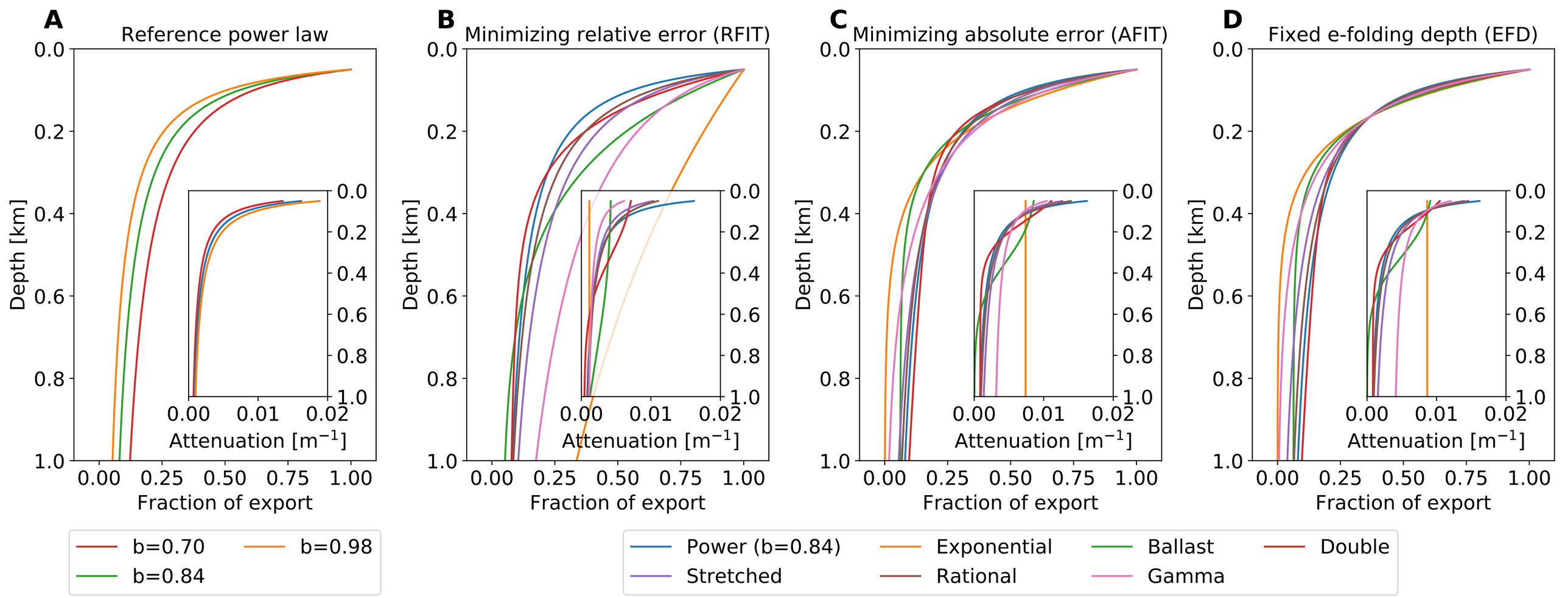
A
Reference power law
B
Minimizing relative error (RFIT)
C
Minimizing absolute error (AFIT)
D
Fixed e-folding depth (EFD)
Depth [km]
Fraction of export
Attenuation [m^{-1}]
0.0
0.2
0.4
0.6
0.8
1.0
0.00
0.25
0.50
0.75
1.00
0.01
0.02
b=0.70
b=0.84
b=0.98
Power (b=0.84)
Stretched
Exponential
Rational
Ballast
Gamma
Double

Figure 3.

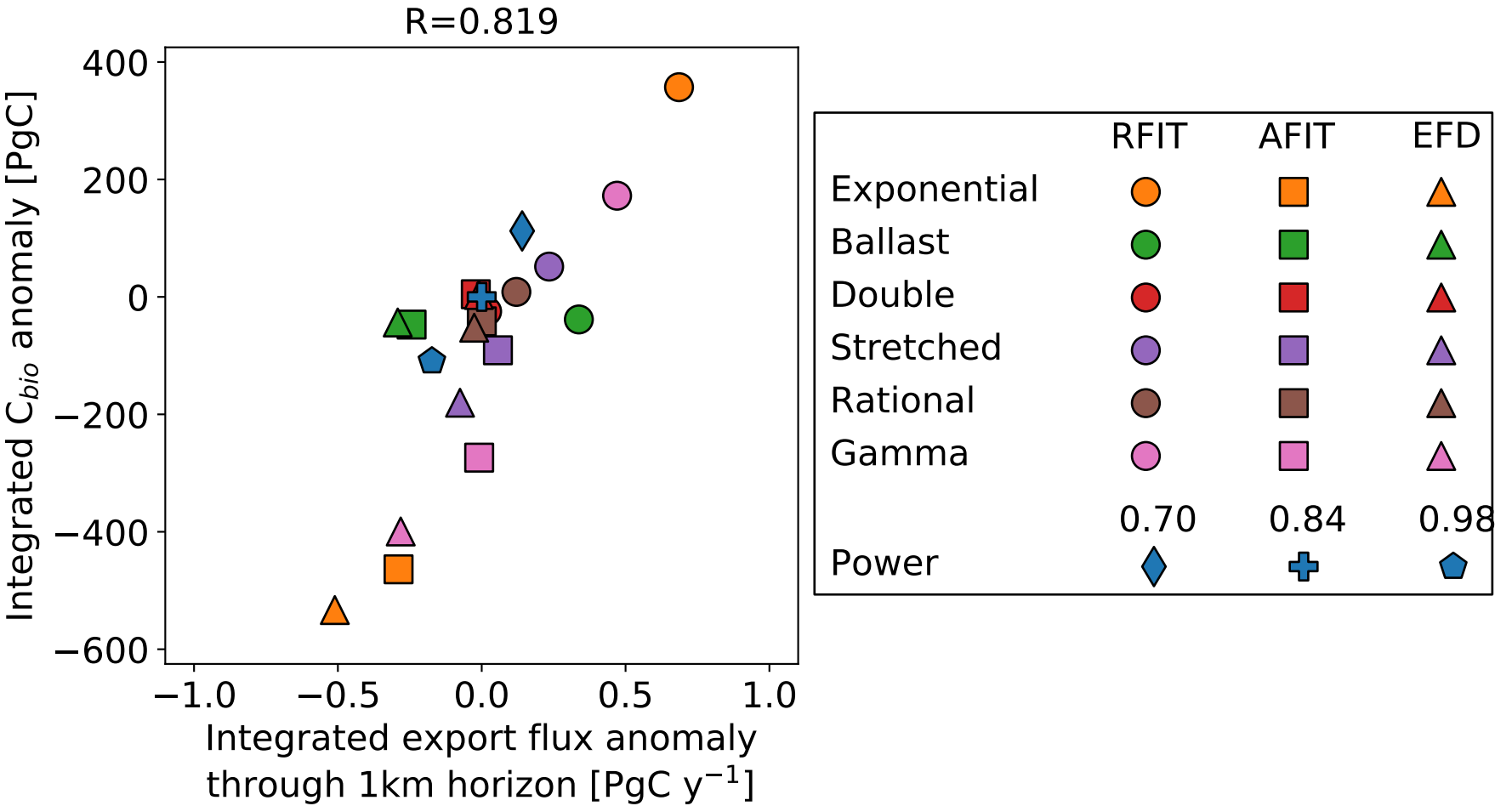
R=0.819
Integrated C_{bio} anomaly [PgC]
400
200
0
−200
−400
−600
−1.0
−0.5
0.0
0.5
1.0
Integrated export flux anomaly
through 1km horizon [PgC y^{-1}]
RFIT
AFIT
EFD
Exponential
Ballast
Double
Stretched
Rational
Gamma
0.70
0.84
0.98
Power

Figure 4.

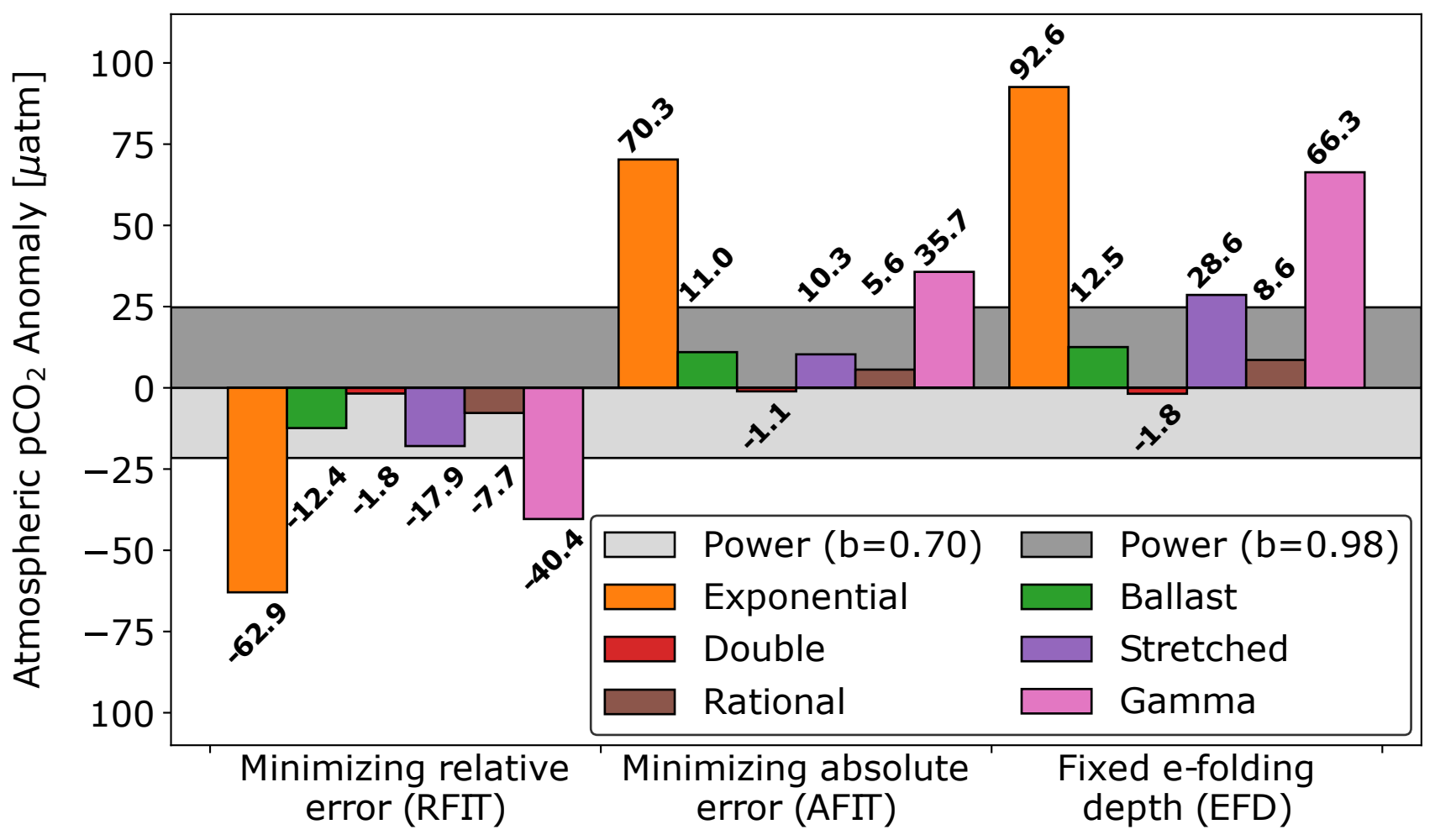
Atmospheric pCO2 Anomaly [μatm]
100
75
50
25
0
−25
−50
−75
100
-62.9
-12.4
-1.8
-17.9
-7.7
-40.4
70.3
11.0
-1.1
10.3
5.6
35.7
92.6
12.5
-1.8
28.6
8.6
66.3
Power (b=0.70)
Exponential
Double
Rational
Power (b=0.98)
Ballast
Stretched
Gamma
Minimizing relative error (RFIT)
Minimizing absolute error (AFIT)
Fixed e-folding depth (EFD)